Molecular Vision 2017; 23:416-430 <http://www.molvis.org/molvis/v23/416>
Received 27 December 2016 | Accepted 5 June 2017 | Published 7 July 2017

Origins of the phototransduction delay as inferred from stochastic and deterministic simulation of the amplification cascade

Alexander Yu Rotov,[1,2] Luba A. Astakhova,[1] Michael L. Firsov,[1] Victor I. Govardovskii[1]

[1]Institute for Evolutionary Physiology and Biochemistry, Russian Academy of Sciences, St. Petersburg, Russia; [2]Peter the Great St. Petersburg Polytechnic University, St. Petersburg, Russia

Purpose: To identify steps of the phototransduction cascade responsible for the delay of the photoresponse.
Methods: Electrical responses of fish (*Carassius*) cones and *Rana ridibunda* frog rods and cones were recorded with a suction pipette technique and as an aspartate-isolated mass receptor potential from isolated perfused retinas. Special attention was paid to sufficiently high temporal resolution (1-ms flash, 700 Hz amplification bandpass). Stochastic simulation of the activation steps from photon absorption to the formation of catalytically active phosphodiesterase (PDE) was performed. In addition, a deterministic mathematical model was fit to the experimental responses. The model included a detailed description of the activation steps of the cascade that enabled identification of the role of individual transduction stages in shaping the initial part of the response.
Results: We found that the apparent delay of the photoresponse gets shorter with increasing stimulus intensity and reaches an asymptotic value of approximately 3 ms in cones and greater than or equal to 10 ms in rods. The result seems paradoxical since it is suggested that the delay occurs in the chain of steps from photon absorption to the formation of active transducin (T*) which in cones is, on average, slower than in rods. Stochastic simulation shows that actually the steps from photon absorption to T* may not contribute perceptibly to the delay. Instead, the delay occurs at the stage that couples the cycle of repetitive activation of T by rhodopsin (R*) with the activation of PDE. These steps include formation of T* (= T_{α}GTP) out of $T_{\alpha\beta\gamma}$GTP released from the activation cycle and the subsequent interaction of T* with PDE. This poses a problem. The duration of an average cycle of activation of T in rods is approximately 5 ms and is determined by the frequency of collisions between R* and T in the photoreceptor membrane. The frequency is roughly proportional to the surface packing density of T in the membrane. As the packing density of PDE is approximately 12 times lower than that of T, it could be expected that the rate of the T*–PDE interaction were an order of magnitude slower than that of R* and T. As modeling shows, this is the case in rods. However, the delay in cones is approximately 3 ms which could be achieved only at a T*–PDE interaction time of less than or equal to 5 ms. This means that either the frequency of the collisions of T* and PDE, or the efficiency of collisions, or both in cones are approximately ten times higher than in rods. This may be a challenge to the present model of the molecular organization of the photoreceptor membrane.
Conclusions: The delay of the photoresponse is mainly set by the rate of interaction of T* with PDE. In cones, the delay is shorter than in rods and, moreover, shorter than the duration of the cycle of repetitive activation of T by R*. This poses a problem for the present model of diffusion interaction of phototransduction proteins in the photoreceptor membrane.

The photoresponses of vertebrate rods and cones exhibit a delay phase that in amphibians lasts from approximately 3 ms to greater than 10 ms. This is not surprising as the conversion of the photon absorption by rhodopsin into the cell's electrical response is mediated by a multistep biochemical cascade. The delay is tacitly attributed to the reactions that lead to the generation of the active transducin (*T**) and phosphodiesterase (PDE*) [1-3]. Activation of transducin by the active rhodopsin state (R* = Metarhodopsin II) proceeds via at least five steps (Figure 1). At step 1, R* meets an inactive transducin trimer ($T_{\alpha\beta\gamma}$GDP) and binds it. Rhodopsin and transducin are thought to freely move in the photoreceptor membrane colliding at the rate of approximately 6,000 s^{-1}, and on average, one of 30 collisions is productive, that is, leads to the formation of the R*–$T_{\alpha\beta\gamma}$GDP complex at the rate of approximately 200 s^{-1} [3]. At step 2, the R*-bound $T_{\alpha\beta\gamma}$GDP complex releases GDP thus vacating a binding site for GTP. At step 3, GTP binds to the site. At step 4, the R*–$T_{\alpha\beta\gamma}$GTP complex dissociates. After dissociation, free R* can initiate the next cycle of activation. Meanwhile, $T_{\alpha\beta\gamma}$GTP dissociates into $T_{\beta\gamma}$ and T_{α}GTP (step 5). T_{α}GTP is the active form of transducin (T*) that at step 6 binds to phosphodiesterase and activates it. Activation of PDE translates into the electrical response of the photoreceptor via cGMP hydrolysis and closure of the cGMP-gated ionic channels (CNGCs) in the plasma membrane of the outer segment (reviewed in [3]).

The duration of a single cycle of activation is the time between R* initiating the chain (states 1–4) at state 1 and its release from $R^*T_{\alpha\beta\gamma}GTP$ at state 4, thus the time per single activation $t_t = t_1 + t_2 + t_3 + t_4$ (Figure 2). Keeping in mind

Correspondence to: Victor Govardovskii, IEPHB RAS, 44 Thorez prospect 194223 St. Petersburg, Russia; Phone: (7)-(812)-5504989; FAX: (7)-(812)-5504989; email: vgovardovski@yahoo.com

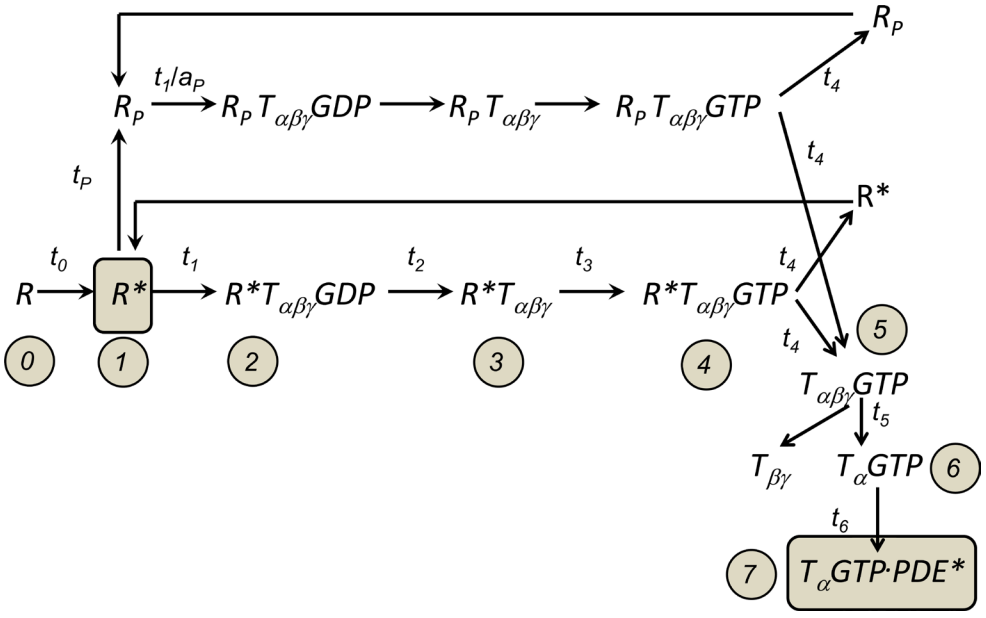

Figure 1. Scheme of the initial steps of the phototransduction cascade, starting from photon absorption by rhodopsin (*R*, state *0*) and proceeding to the formation of active PDE (the $T_\alpha GTP \times PDE^*$ complex, state 7). Encircled numbers designate the intermediate states of the components of the cascade. t_0 to t_6 are time constants of corresponding transitions. At the transition from state 4 to 5, *R** is released from transducin and returns to state 1 initiating a new loop of T activation. There also is a parallel path of activation via the cycle driven by rhodopsin partially inactivated by phosphorylation (R_p). It is suggested that phosphorylation slows the transition from state 1 to state 2 (t_1) by a factor a_p greater than 1; all following reactions are thought to be unaffected.

the inherent randomness of all molecular events, the *average* rate of repetitive production of active T* is $v_{RG} = 1/t_{cycle}$ where the t_{cycle} is the *average* of the individual t_is. The time interval between the photon absorption and the appearance of the first PDE* is equal to the total durations of steps 1 to 6, $t_1 + t_2 + t_3 + t_4 + t_5 + t_6$, plus a certain delay t_0 needed for formation of Meta II from early photointermediates, plus other possible delays between $T_\alpha GTP$–PDE binding and formation of the active PDE*. Thus, the delay time should be $t_d \geq t_0 + t_1 + t_2 + t_3 + t_4 + t_5 + t_6$. Here t_d is an arbitrarily chosen time point at which the minimum deviation of PDE activity from its dark level can be detected. In addition, extra steps may exist between the formation of $T_\alpha GTP \times PDE$ and the start of the full-speed PDE* production (shown in Figure 2 with the bent line) [1-3].

Pugh and Lamb [1,2] suggested that the time course of the flash-induced PDE activity could approximately be described by a delayed ramp with a certain effective delay $t_{eff} > t_d$ (the red curve in Figure 2). Then the time course of the cGMP hydrolysis (and thus, the electrical response *r(t)*) is predicted to be a squared parabola starting at t_{eff}:

Equation 1

$$r(t) = \frac{1}{2}\Phi \cdot V_{RE} \cdot \beta_{sub} \cdot n_{cG} \cdot (t - t_{eff})^2 \qquad t \geq t_{eff}$$

Here, Φ is the number of activated rhodopsins, v_{RE} is the steady rate of PDE activation, β_{sub} is the catalytic activity of a single PDE subunit per outer segment cytoplasmic volume, and n_{cG} is the Hill coefficient of the cGMP channel activation. Further, it was argued that the effective delay of the photoresponse is a bit longer than t_{eff} of PDE activation, but the difference is supposed to be small ([3], see also the Discussion section). In addition, the coupling between T* and PDE* may be imperfect due to diffusion limitations; therefore, in general $v_{RE} < v_{RG}$ [4]. Later, it was argued that in reality the coupling efficiency is close to unit [3]. Therefore, we assume $v_{RE} = v_{RG} = 1/t_{cycle}$ and use v_{RE} throughout, except the cases when the treatment specifically refers to the chain t_1–t_4. In addition, in line with [3], we consider two PDE* subunits as separate functional units since they are enzymatically equivalent and can be activated independently [5,6].

The parabolic fitting of the initial part of the photoresponse in the form of Equation (1) is widely used to extract the amplification and the effective delay from the experimental recordings. However, t_{eff} is not the real transduction delay t_d (Figure 2). In addition, the rate of the PDE* production (and thus, amplification) is set by t_{cycle} that comprises part of t_d and t_{eff}. This means that the amplification and delay parameters are interrelated. Thus, it is of significant interest to identify and quantify the steps of the activation chain that shape the delay and amplification. This may shed light on the kinetics of the underlying reactions (t_1 *to* t_6) and further our understanding of the molecular mechanics of the cascade activation.

To do this, we collected data on the photoresponse delays in frog (*Rana ridibunda*) and fish (*Carassius*) cones and frog rods specifically focusing on high time resolution and low noise. We found that in the cones the delay t_d is approximately 3 ms and in the rods is greater than or equal to 10 ms. Then we performed stochastic simulation of the reactions that lead to the production of active phosphodiesterase (PDE*). Contrary to expectations, we found that the delay of the averaged photoresponse is shorter than the average duration of the sum of the activation steps. For instance, the time from the appearance of R^* to dissociation of the $R^*–T_{\alpha\beta\gamma}GTP$ complex (steps 1 to 4 in Figure 1, Figure 2) obtained from many averaged simulations (multiphoton responses) is shorter than the average t_{cycle}. It depends on the relative durations of the steps. The delay of the appearance of T* is longest when all four steps comprising the cycle are of equal duration (that is, $t_1 = t_2 = t_3 = t_4 = 1/4\ t_{cycle}$) but is substantially shorter than the sum of the individual steps ($t_1 + t_2 + t_3 + t_4$). If any of the steps is dominant (slowest), then the delay of the average decreases and may approach zero. The main delay in PDE* production occurs at steps 5 and 6, that is, during the dissociation of the $T_{\alpha\beta\gamma}GTP$ trimer into $T_{\beta\gamma} + T_\alpha GTP$ and $T_\alpha GTP–PDE$ binding. We also performed a model simulation of complete photoresponses using a continuous deterministic description of the steps *t0–t6*; the result was in exact agreement with the results of the stochastic simulation. We determined the restrictions that must be applied to relevant parameters to reproduce experimental responses. It appeared that the average time of $T_{\alpha\beta\gamma}GTP$ to the $T_\alpha GTP \times PDE^*$ transition ($t5 + t6$) in cones must be shorter than or equal to the average time of repetitive $T_{\alpha\beta\gamma}GTP$ production (t_{cycle}). This is quite surprising because the surface packing density of *PDE* in the photoreceptor membrane in rods and cones is roughly an order of magnitude lower than that of *T* [3,7]. Thus, it is expected that the frequency of diffusion collisions between *T** and *PDE* would

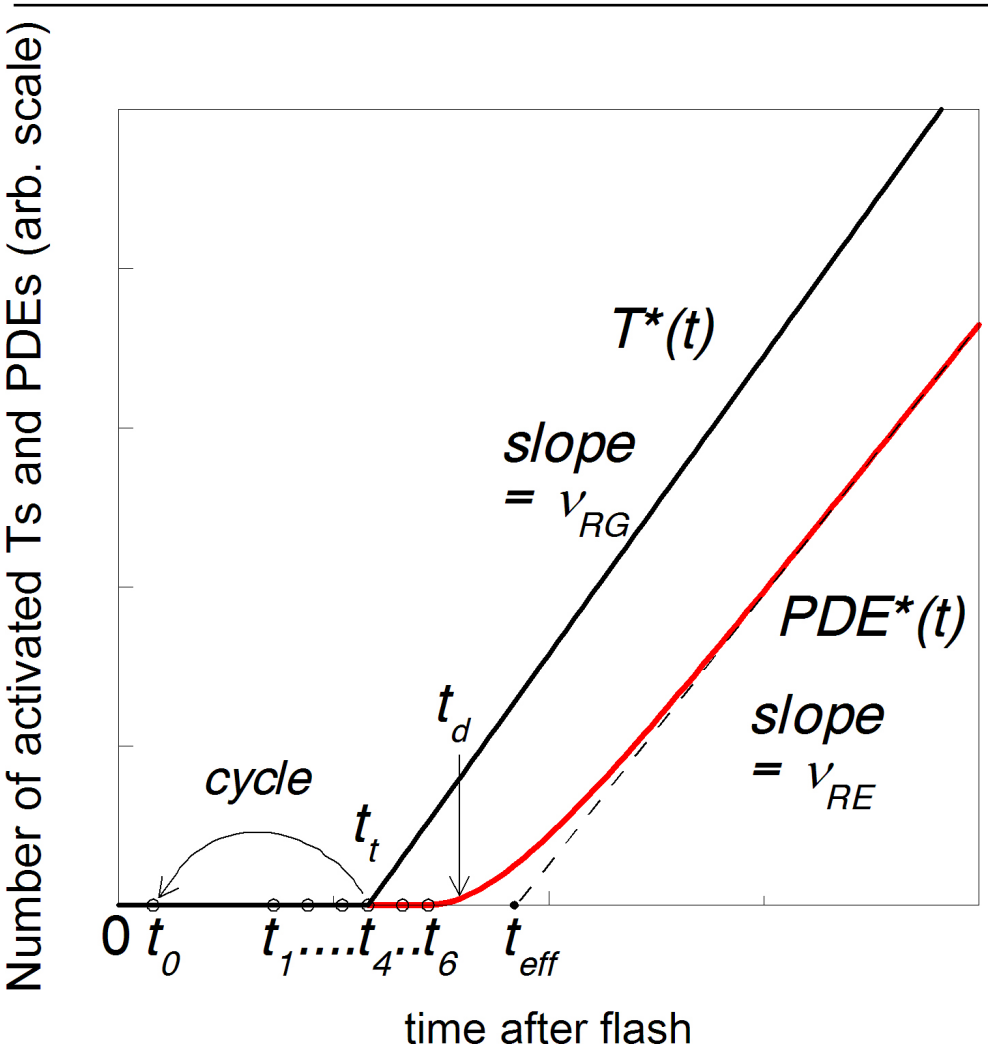

Figure 2. Time course of the production of active transducin (T*) and phosphodiesterase (PDE*) (modified from [1-3]). Times from t_0 to t_6 represent the durations of corresponding transitions in Figure 1 (state 0 to state 1, state 1 to state 2, etc.). The straight line initiating from t_4 shows the time course of T* production, at the rate of ν_{RG}. The first PDE* would ideally appear at t_6. The bent red line shows a more realistic approximation that may result from the extra delay between T*–PDE binding and activation of PDE. ν_{RE} is the steady rate of PDE* production achieved after an effective delay t_{eff}. In accordance with [3], we further assume $\nu_{RE} = \nu_{RG} \cdot t_d > t_6$ is placed, rather arbitrarily, as the delay time when the minimum deviation of PDE* from its dark level can be detected.

also be an order of magnitude lower than that between R^* and T.

METHODS

Animals and preparations: Adult *Rana ridibunda* frogs were caught in the wild in southern Russia, and *Carassius* fish were obtained from local hatcheries. The frogs were kept for up to 6 months with free access to water at 10 to 15 °C on a natural day/night cycle and fed mealworms. Fish were kept in aerated aquaria at room temperature (near 20 °C) at a 12 h:12 h light-dark cycle and fed dry fish food. Animals were treated in accordance with the European Communities Council Directive (24 November 1986; 86/609/EEC), ARVO Statement for Use of Animals in Research, and the protocol approved by the local Institutional Animal Care and Use Committee. Before the experiment, the animals were dark-adapted overnight. Eyes were enucleated and the retinas extracted under dim red light. All further procedures were conducted at infrared (IR) TV surveillance.

Electrical recordings: Suction pipette recordings were performed from frog rods attached to small pieces of the retina, and from attached or isolated fish cones, sucked in configuration outer segments in. The specific details of the suction setup design and functioning have been previously described [8,9]. The light stimulation system consisted of two independent channels based on high-output light-emitting diodes (LEDs) with λ_{max} = 519 and 632 nm. By comparing sensitivities at the two wavelengths, it was possible to discriminate spectral classes of the photoreceptors (red-sensitive versus green-sensitive versus blue-sensitive cones in the goldfish and red rods versus green rods in the frog). Stimulus intensity was controlled by switchable neutral-density (ND) filters and LED current. The shortest flash duration was 1 ms. Responses were low-pass filtered at 700 Hz (eight-pole analog Bessel filter) and recorded at 1-ms digitization intervals. All recordings were further shifted by −1 ms to account for the delay introduced by the filter. Digital filtering was not applied. Flash intensity was calibrated using a Burr-Brown OPT-301 integrated optosensor (Tucson, AZ) and regularly checked during the experiments on individual rods using the Poisson statistics of responses to weak flashes [10]. Rods were video recorded to measure their size, so the stimulus intensity could be specified as fractional bleach per flash (for flashes) or per second (for continuous backgrounds). Data acquisition, stimulus intensity, and timing were controlled by National Instruments (Austin, TX) hardware and LabView software (Austin, TX).

In addition, frog and *Carassius* cone responses were recorded across the isolated retina placed in an Ussing-type perfusion chamber. The electroretinogram (ERG) *b*-wave was suppressed and the receptor potential (RP) isolated by adding 12 mM sodium aspartate to the perfusion solution. The illuminating system consisted of three independent light channels, one with a 525 nm LED and two with white LEDs. This allowed the application of background light and independently controlled stimulus color with appropriate filters. Specifically, the responses of the frog red-sensitive cones were recorded with orange stimuli (cut-off at 600 nm) on a 525-nm LED steady background that suppressed the rod response. For the *Carassius* retina, a 640-nm cut-off filter was used that selectively stimulated red-sensitive cones. Light intensity was calibrated with a Burr-Brown OPT-301 opto-sensor, and additionally by measuring rhodopsin bleaching in frog rods with microspectrophotometry. In the ERG rig, the shortest flashes were 1 ms, and digitization was at 0.5 ms. Further frequency filtration was as in the suction rig. The ERG rig was controlled via the PCI-DAS-1602 I/O card (Measurement Computing, Norton, MA). The controlling program was custom written in the laboratory using Microsoft Visual Basic 96 and Measurement Computing Universal Library.

Solutions: Main Ringer solution used to record from frog photoreceptors (further referred to as normal) contained NaCl 90 mM, KCl 2.5 mM, $MgCl_2$ 1.4 mM, $CaCl_2$ 1.05 mM, $NaHCO_3$ 5 mM, HEPES 5 mM, glucose 10 mM, and EDTA 0.05 mM; pH was adjusted to 7.6. Stock aspartate solution (120 mM) was added to the perfusion solution to the final concentration of 12 mM, when needed. All chemicals were from Sigma-Aldrich (St. Louis, MO). Temperature was held at 17 to 19 °C. The perfusion solution for recording from the fish cones contained NaCl 102 mM, KCl 2.6 mM, $MgCl_2$ 1 mM, glucose 5 mM, $CaCl_2$ 1 mM, $NaHCO_3$ 28 mM, HEPES 5 mM, and bovine serum albumin (BSA) 50 mg/l; pH was adjusted to 7.8–8.0.

Mathematical modeling:

Stochastic simulation—To account for the randomness of the activation events, we performed stochastic simulation of the reactions that lead to the production of the active phosphodiesterase ($PDE^* = T_\alpha GTP \times PDE$, Figure 1). We used the algorithm suggested by Gillespie [11] that is widely used for modeling the variability of single-photon responses, most recently in [12]. A single cycle of the program generated a series of states from 0 to 7 (Figure 1) separated by time intervals t_0 to t_6 (Figure 2). Each interval varied randomly according to an exponential distribution [4,11-13], with the corresponding average t_0 to t_6 time constants. Each R^* released at state 4 initiated a new loop of activation events,

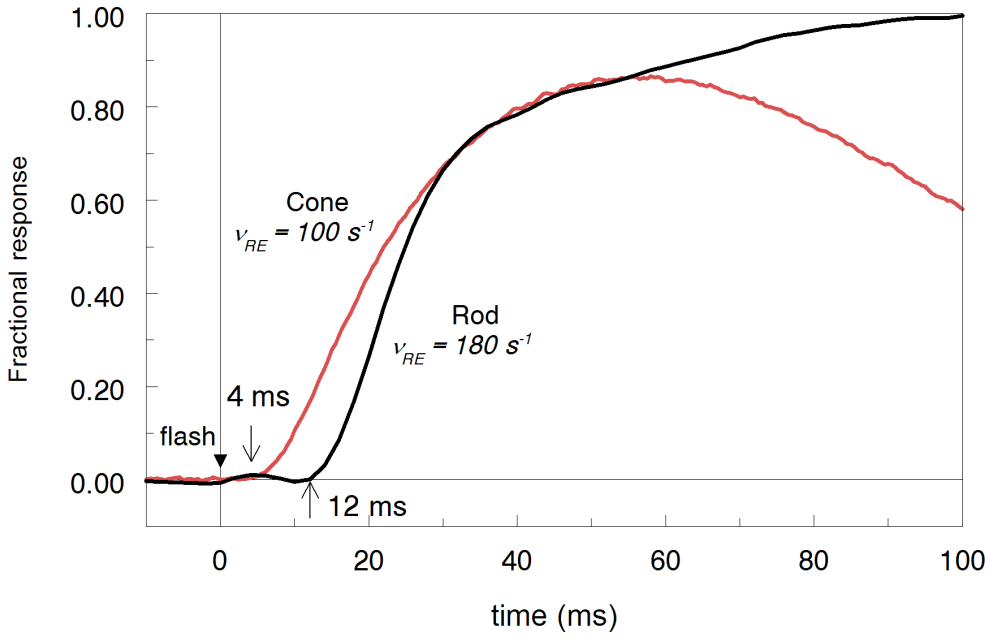

Figure 3. Delay of the response to bright flashes in cones is shorter than in rods. Suction pipette recordings from *Carassius* red-sensitive cone and from *Rana ridibunda* rhodopsin rods are shown. Here and throughout, experimental photoresponses are expressed as fractional with respect to the dark current (for suction recordings) or to the amplitude of the saturated response (for transretinal recordings). Recording bandpass, digitization, and flash duration are as indicated in Methods. Flash intensity is expressed as fractional bleach: Cone, $1.4 \cdot 10^{-4}$; Rod, $3.9 \cdot 10^{-5}$. Rates of the cascade activation v_{RE} shown near the curves are derived from the minimum essential model (MEM) fitting.

now starting from P_1, and the cycle was repeated, for example, 100 times. A large number of sweeps, each consisting of 100 activation loops, was repeated and summed to obtain the response to many photons. Computations were performed with a program written in Microsoft Visual Basic 96.

Deterministic model—For modeling the entire photoresponse, we used a deterministic model consisting of a set of differential equations. The model was described in [14] and named there the minimum essential model (MEM). However, in the MEM the activation of PDE by R* is considered a single-step reaction with an adjustable delay and rate v_{RE}. To account for the multistep nature of cascade activation, the MEM was supplemented with extra front-end equations (see the Equations section) that provided a detailed description of the Figure 1 steps t_0 to t_6, similarly to [15]. The model treats the outer segment as a well-stirred volume. We call it the extended MEM (E-MEM). The model was implemented in MathCad (MathSoft, Cambridge, MA).

RESULTS

Figure 3 shows the main experimental finding that prompted this work. It appeared that the delay of the photoresponse in cones is substantially shorter than that in rods, while, at least in this particular case shown in Figure 3, the speed of the activation of the phototransduction cascade in the cone is half of that in the rod. Moreover, although the amplification in the best cones may be as high as in the rods [14], on average, it is two to four times lower [14,16,17]. It apparently contradicts the simplified treatment of the phototransduction delay shown in Figure 2. The rate of steady production of T* and PDE* v_{RE} is inverse to the total duration of steps 1 to 4 ($t_{cycle} = t_1 + t_2 + t_3 + t_4$, Figure 1 and Figure 2). Then one could expect that cone $t_d \geq$ rod t_d (assuming, of course, that the interaction between *T** and *PDE* via steps 5 to 6 occurs at the same rate in the rods and cones).

In each individual single-photon response, the first PDE* appears at $t_0 + t_1 + t_2 + t_3 + t_4 + t_5 + t_6$ (Figure 2). However, the reactions of single molecules are subject to stochastic fluctuations, and each $t_0 \ldots t_6$ vary randomly among the activation events. To account for this effect, we performed a stochastic simulation of the reactions that lead to the production of active phosphodiesterase ($PDE^* = T_\alpha GTP \times PDE$; see Methods). As an example, Figure 4A shows two series of responses, each initiated by a single photon. Notice that in the graph the values for $T_{\alpha\beta\gamma}GTP$ (state 5) correspond to the total number of the molecules produced up to the corresponding time point; the number of $T_{\alpha\beta\gamma}GTP$s existing at this moment is lower due to its further processing via states 6 and 7. The figure shows that the delays in the production of the first $T_{\alpha\beta\gamma}GTP$ and PDE* are different in the two program sweeps, as expected from the random process.

Summing multiple sweeps (which is equivalent to the response to many photons) reveals that there is actually no pure delay in the activation of the cascade (Figure 4B). This is

because there always is a probability that, due to the randomness of the process, the first active T* or PDE* appears almost immediately after a photon absorption. Remarkably, the time of the R to R* transition t_0, which is 1 ms in rods [18] and 0.5 ms in cones [19], does not contribute perceptibly to the delay (see the initial part of the T* curve in Figure 4B). In addition, although in the example simulation the average duration of the cycle of activation $t_{cycle} = t_1 + t_2 + t_3 + t_4 = 5$ ms is equal to the duration of the final steps 5 and 6 ($t_5 + t_6$), the main delay of PDE* production occurs at the two latter steps (cf. the curves for T* and PDE* in Figure 4B).

More detailed analysis of the activation cycle t_1 to t_4 shows that the delay depends not on the entire duration of the cycle ($t_1 + t_2 + t_3 + t_4$) but on the presence of a single dominant (slowest) reaction in it. We fixed the total duration of the cycle at 5 ms, close to that determined in direct biochemical measurements [20], and varied the contribution of the individual steps to the total duration. If a single step is rate-limiting, then the delay of the (average) $T_{\alpha\beta\gamma}GTP$ production is much shorter than the average $t_1 + t_2 + t_3 + t_4$ and may approach zero (Figure 5, red symbols). However, if all four intermediate steps are of equal duration, then the delay of about 1 ms is the longest but still substantially shorter than $t_1 + t_2 + t_3 + t_4$ (Figure 5, black symbols). The results of the stochastic simulation are in agreement with the prediction of the deterministic continuous model based on Equations (1e) to (5e) with $t_5 = \infty$ (smooth lines through the simulated points).

Comparing the theoretical predictions with delays measured experimentally meets a problem, though. As seen in Figure 4, there is no pure delay in the multiphoton *PDE*(t)* response. The delay t_d marked in Figure 2 is arbitrary and depends on the ability to detect the minimum deviation of PDE* from its prestimulus level. Further, PDE activity translates into the electrical response via a sequence of reactions that greatly modify the shape of the response and may introduce extra delays. Estimating the delay of the experimental responses may also suffer from arbitrariness. The delay depends on the ability to detect the minimum deviation from the prestimulus dark current level in the averaged responses. The apparent delay depends on the steepness of the curve and thus decreases with increasing stimulus intensity (Figure 6). Fortunately, at a certain intensity the steepness of the response front saturates, and the delay reaches the minimum [21,22]. Determining this minimum delay value depends on the experimental noise. To avoid ambiguity, we define the start of the response as the first post-stimulus point that lies at or beyond the 0.0025 fractional response, provided that it is also above two standard deviations of the prestimulus record stretch.

The average values of delays in rods and cones in the experimental recordings are summarized in Table 1. To determine what parameters of individual reactions in the activation chain are compatible with the observed photoresponse delay, a complete phototransduction model was necessary. A stochastic simulation can easily be run to the stage of production of PDE*. However, simulating further processes this way

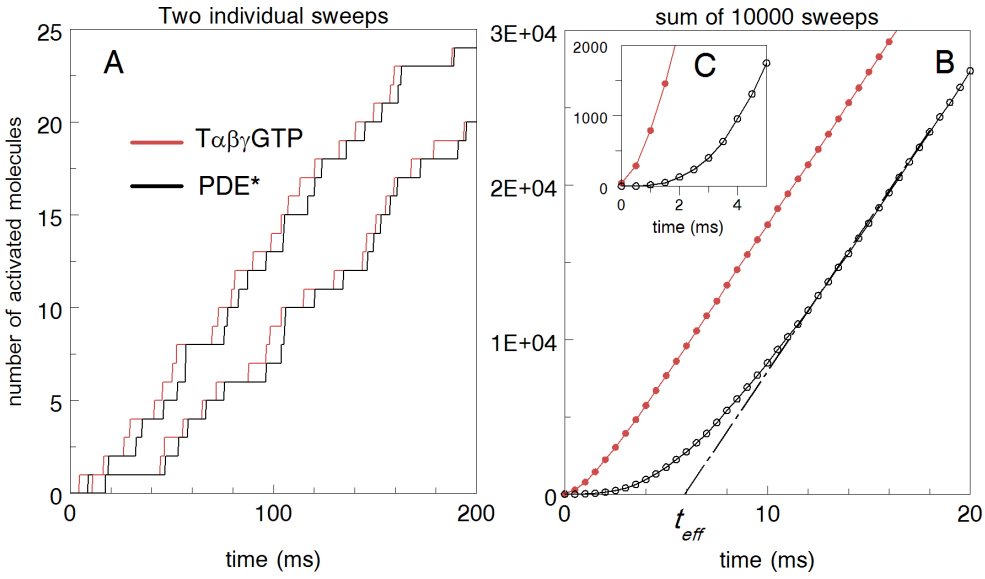

Figure 4. Time courses of active transducin (*T**) and phosphodiesterase (*PDE**) determined with a stochastic simulation. **A**: Two independent repetitive cycles of reactions show the time course of accumulated concentrations of *Tαβγ-GTP* and *PDE** after the activation of single rhodopsin. **B**: The whole cycle is repeated 10,000 times to get the result summed over many quanta. Time constants (in ms) are $t_0 = 1$, $t_1 = 4.7$, $t_2 = 0.1$, $t_3 = 0.1$, $t_4 = 0.1$. Total duration of the activation cycle ($t_1 + t_2 + t_3 + t_4 = 5$ ms) was fixed according to biochemical data on the rate of T activation in frog rods (about 200 s^{-1} [19]). $t_5 = 2.5$; $t_6 = 2.5$. t_0 is the time of Meta II production in frog rods [17].

is impractical. It has been shown that the average of many stochastic simulations is equivalent to the solution of a set of deterministic differential equations each describing the corresponding reaction [11,13]. Thus, to quantitatively analyze the factors that shape the phototransduction delay we used the MEM of phototransduction [14] updated to the E-MEM (see the Methods and Equations sections). For fitting, we started from the values of the parameters of the rod and cone cascade determined in our previous work [14]. Further, the fit was refined by trial and error, and the quality of the fit was judged by computing the coefficient of correlation between the experimental and model responses. A sample fit to a frog rod and cone photoresponse is shown in Figure 7A,B. The fits in Figure 7 yield $r = 0.9997$ for cones and $r = 0.9987$ for rods. The parameters of the fits in Figure 7 are given in Table 2.

DISCUSSION

Definition and experimental determination of the phototransduction delay: The fact that the (apparent) delay of the flash response in the fish cones is shorter than in the rods was observed recently in [17]. Actually, the photoresponse delays were measured for decades, and a reference list would include more than 30 directly relevant papers. However, it is hard to compare most of the old results with recent data because of different experimental procedures and different definition(s) of the delay. The main shortcomings of the classical works (in the context of the present problem) were insufficiently wide recording bandpass and/or too long stimuli. Only a few papers are free of this flaw. Cobbs and Pugh [21], applying very intense brief flashes, found an irreducible delay of approximately 7 ms in salamander rods. However, such bright flashes (up to 10% rhodopsin bleach) should evoke a noticeable early receptor potential/current (ERP/ERC) that would contaminate the initial part of the response. Thus, the 7-ms delay in rods may well be an underestimate. The contamination by the ERC is clearly seen in recordings from salamander cones and rods in [22]; therefore, the moment of the beginning of the cGMP-gated photoresponse cannot be determined with certainty. The value of the delay reported by the authors (approximately 8 ms) is derived from a certain fitting to the rising phase of the response and is a clear overestimate. Yet Hestrin and Korenbrot's general conclusion [22] was that the values for the delay are nearly identical in rods and cones. Delays reported in [14] are not experimental values but are

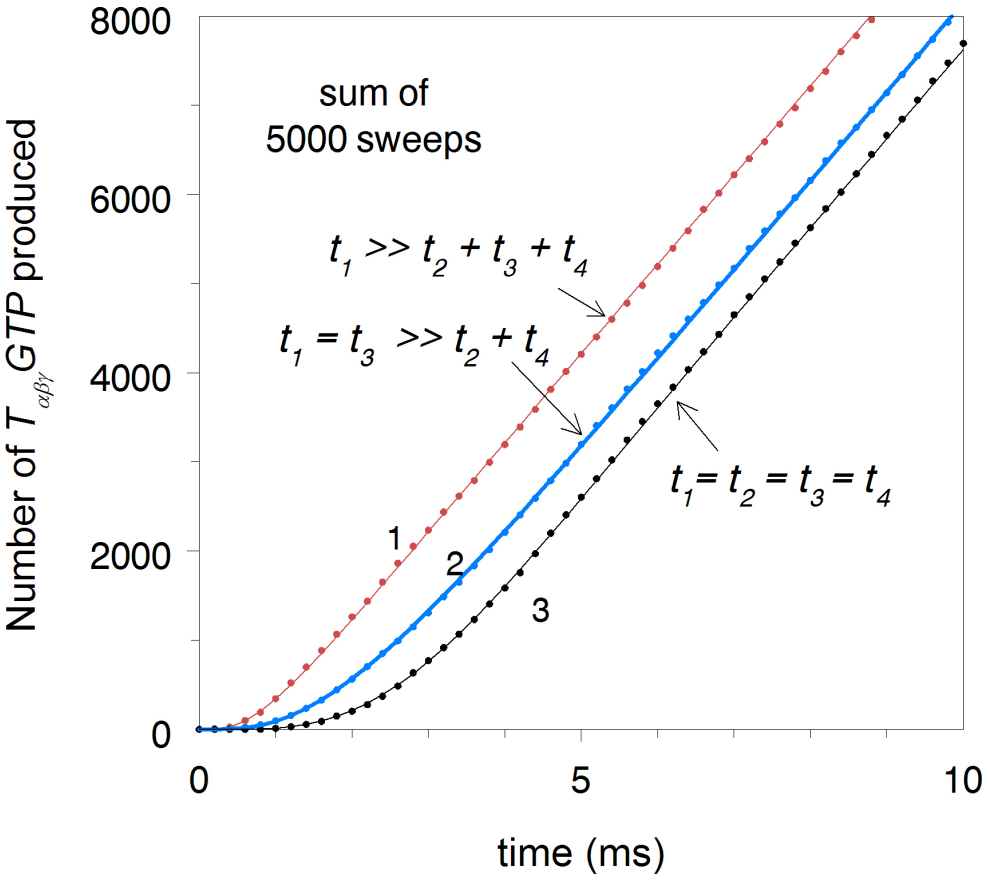

Figure 5. Effect of the number of rate-limiting steps within the activation cycle on the $T_{\alpha\beta\gamma}GTP$ production delay. A stochastic simulation of the activation cycle was performed fixing the total duration of the cycle ($t_1 + t_2 + t_3 + t_4 = 1/v_{RE} = 5$ ms, Figure 1 and Figure 2) but varying the contributions of individual steps to it. Curve 1, $t_1 = 4.7$ ms, $k_2 = k_3 = k_4 = 0.1$ ms. Curve 2, $k_1 = k_2 = 2.4$ ms, $k_3 = k_4 = 0.1$ ms. Curve 3, $k_1 = k_2 = k_3 = k_4 = 1.25$ ms. Smooth lines through the dots show the results of continuous deterministic computations using the same parameters.

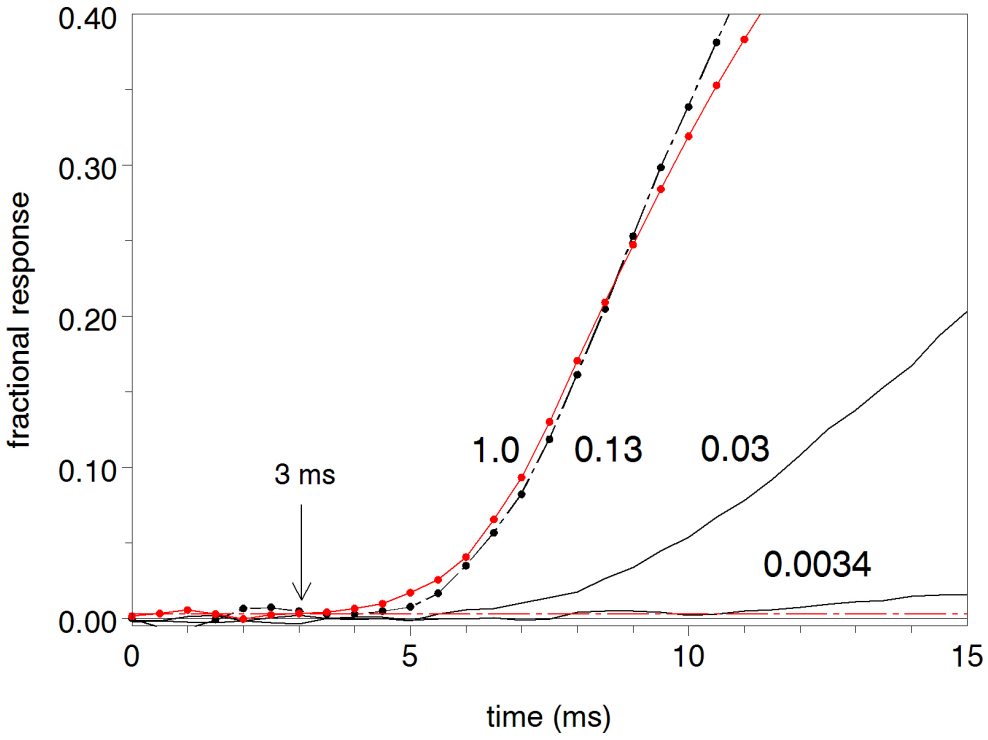

Figure 6. Dependence of the apparent delay on the stimulus intensity in cones. Trans-retinal recordings of the aspartate-isolated receptor potential of frog red-sensitive cones. Each trace is the average of 100 to 500 responses. Green (525 nm) background illumination was applied to saturate the rods' responses, and an orange (longer than 600 nm) 1-ms flash was used as the stimulus for the cones. The beginning of the flash is at 0.0 s. Experimental recordings are shifted by –1 ms to account for the analog filter delay. The horizontal red dot-dash line marks the 0.0025 criterion level. The numbers near the traces show the relative flash intensities. Intensity 1.0 corresponds to 1.4×10^{-4} fractional bleach per flash.

the fitting parameters of a model in which the activation of PDE was considered a linear function starting abruptly with an adjustable delay after the stimulating flash. Their relation to the experimental delays (as e.g., in Figure 3 and Figure 7) and to the scheme shown in Figure 2 is unclear. Facing this uncertainty, we had to make a series of experiments especially dedicated to reliably estimating photoresponse delays in rods and cones.

As we show, within the accepted scheme of phototransduction there is no distinct delay between a flash and (averaged) cGMP-gated photoresponse. However, the multistep sequence of reactions that couple photon absorption with the CNGC closure results in a steep initial phase of the response. It may follow a high-order polynomial function of time making an impression of a true delay [1,21] (Figure 3 and Figure 5). The shortest measureable latency is then determined by the ability to detect a minimum deviation in the cell's current from the dark level. To avoid ambiguity, we define the start of the response as the first post-stimulus point that lies at or beyond the 0.0025 fractional response, provided that it is also higher than two standard deviations of the prestimulus record stretch. In addition to providing a fixed reference point, the criterion also takes into account the experimental noise. Recordings that did not meet the criterion were excluded from further processing.

Thus defined, the delay still clearly depends on the intensity of the stimulus (Figure 6). However, due to limitations within the biochemical cascade and electrical filtering by the cell membrane, the delay at high intensities saturates and reaches a certain minimum value which is approximately 3 ms in *Carassius* and frog cones and approximately 10 ms in frog rods (Table 1). There is no statistically significant difference between the delays obtained with single-cell suction recordings and trans-retinal recordings of the mass receptor potential.

Rate-limiting and delay-setting steps in the phototransduction cascade: Pugh and Lamb [3] suggested that the total

Table 1. Average transduction delays in frog and *Carassius* rods and cones.

Sample	Frog cone LRP	*Carassius* cone LRP	*Carassius* cone suction	Frog rod suction
Delay, ms mean ± SD	3.9±1.1 (35)	4.4±1.0 (15)	4.8±1.3 (5)	11.3±1 (9)
Min. delay and number of samples	3 (11)	3.5 (4)	4 (3)	9 (2)

LRP, transretinal aspartate-isolated Late Receptor Potential.

transduction delay, from photon absorption to the initiation of the electrical response, can be represented as

Equation 2

$$t_d = t_R + t_G + t_E + t_r + t_B + t_C$$

where t_R is the time between photon absorption and generation of Meta II = R*, t_G is the time from R* to the appearance of T*, t_E is the delay between the buildup of T* and the buildup of PDE*, t_r *i*s the time for cGMP diffusion, t_B is the time for equilibration of cGMP with fast buffer sites in the rod outer segment (ROS), and t_C is the delay of the CNGC gating by cGMP.

As we argue, the simple treatment of the (biochemical) delay as the time between photon absorption and the first *T*–PDE** appearance (t_R + t_G + t_E in Equation (2)) is valid only for individual single-photon responses (Figure 2, Figure 4). For the averaged responses to many photons, the duration of the repetitive cycle of activation of *T** by *R** (t_G) has no relation to the delay whatsoever. Due to the stochastic nature of the events, there always is a probability that the first R*, via a fast chain of random intermediate reactions, would

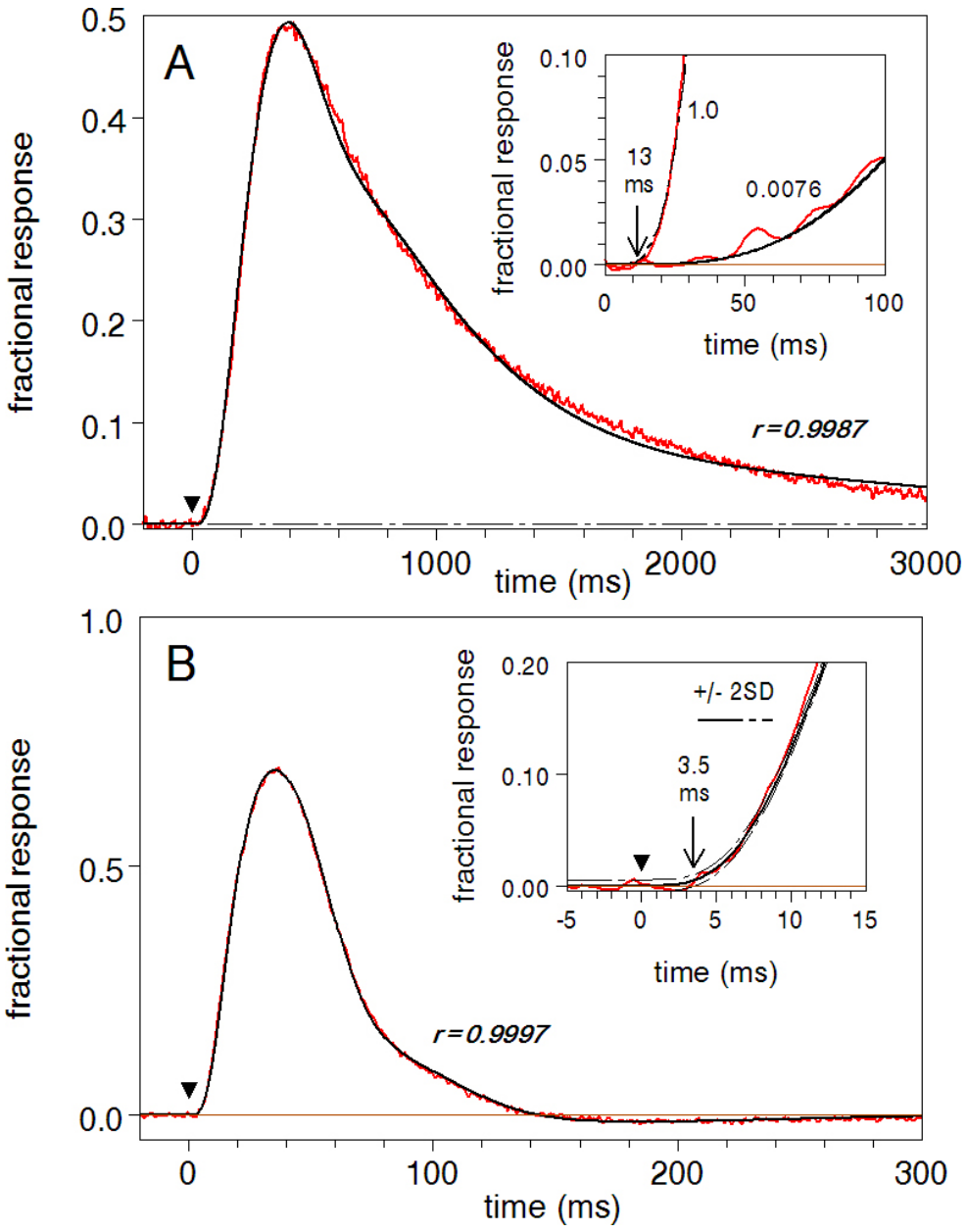

Figure 7. Modeling flash responses of frog rods and red-sensitive cones. The red lines are the experimental recordings; the black lines are the model responses. Black downward triangles show the beginning of a 1-ms stimulating flash. **A**: Suction pipette recording from a frog rod. The insert shows the initial part of the response on an expanded scale. The numbers at the curves indicate the relative intensities of 525-nm flashes. Intensity 1.0 corresponds to the fractional bleach of 1.6×10^{-5} per flash; average of 30 responses. **B**: Transretinal recording of the aspartate-isolated cone receptor potential; rod activity is suppressed by the 525-nm steady background. The stimulus is a 1-ms orange (longer than 600 nm) flash; fractional bleach 6.8×10^{-5} per flash; average of 100 responses. *r* is the coefficient of correlation between the experimental and model curves. Parameters of the fits are given in Table 2.

virtually immediately produce T^*. The exact time course of the average $R^*T_{\alpha\beta\gamma}GTP$ production depends on the presence of a rate-limiting step in the chain (from steps 1 to 4, Figure 1). Provided that the total duration of the activation cycle ($t_{cycle} = t_1 + t_2 + t_3 + t_4$) is kept constant, equal durations of all steps ($t_1 = t_2 = t_3 = t_4$) result in the most threshold-like curve with the longest apparent delay (Figure 5, curve 3). If one of the steps is rate-limiting (say, $t_1 >> t_2 + t_3 + t_4$), then the delay almost vanishes becoming much shorter than the average time of Meta II generation (Figure 5, curve 1).

This idea can easily be understood. Since the total duration t_{cycle} is kept constant, prolonging one of the steps reduces the durations of the three others, eventually making them negligible. Then the entire chain t_1 to t_4 reduces to a single step. The rate-limiting product decays along a single exponential $\exp(-t/t_{cycle})$, and the final product appears as $1 - \exp(-t/t_{cycle})$, with zero delay. The conclusion does not depend on which particular step in the cycle is rate-limiting. This is because steps 1 to 4 comprise a chain of first-order reactions whose output does not depend on the order of the steps. The reasoning is illustrated with a deterministic continuous model of the activation cycle (steps 1 to 4, Equations (2e) to (5e) which is equivalent to the averaged stochastic computations (Figure 5).

The idea that there is a rate-limiting stage in the activation cycle and that this stage is the (average) interval between productive $R^*- T_{\alpha\beta\gamma}GDP$ encounters t_1 (Figure 1 and Figure 2) is supported by experimental data. It was found that the rate of the activation of the cascade increases almost twofold in hemizygous mouse rods with half the normal rhodopsin content, presumably due to reduced molecular crowding in the membrane and the correspondingly increased frequency of R*–T collisions [23]. In addition, the frequency of the R*–T collisions can be decreased tenfold by prolonged light adaptation when 90% of the transducin α- and β-subunits translocate to the inner segment. This causes a corresponding reduction in amplification [24]. Thus, it seems that the R^* to TGDP binding limits the rate of T–PDE activation. In this case, the entire cycle of T activation by R* does not introduce a noticeable delay in the photoresponse (Figure 4 and Figure 5).

Table 2. Parameters of the fits of rod and cone responses shown in Figure 7A,B.

Time constant (s)	Frog rod	Frog cone
t_0	10^{-3} [17]	$0.5\cdot 10^{-3}$ [18]
t_1	$5.1\cdot 10^{-3}$	$4.8\cdot 10^{-3}$
t_2	10^{-4}	10^{-4}
t_3	10^{-4}	10^{-4}
t_4	10^{-4}	10^{-4}
t_5	$1.25\cdot 10^{-2}$	$0.5\cdot 10^{-3}$
t_6	$5.3\cdot 10^{-2}$	$5\cdot 10^{-3}$
t_P	0.565	$2.3\cdot 10^{-2}$
t_{PDE}	0.45	$3.8\cdot 10^{-2}$
t_d	0.435	$2.7\cdot 10^{-2}$

t_0 to t_6 are times of transitions as shown in Figure 1. t_P is the time of R* phosphorylation in darkness, t_{PDE} is the time of PDE* turn-off, and t_d is the dark cGMP turnover time.

The next natural candidate for the delay step in rods looks at the diffusion of cGMP from the outer membrane to the sites of hydrolysis on the disk surface. This would possibly explain a shorter delay in cones because the CNGC and PDE in cones reside in the immediate vicinity within the plasma membrane. The diffusion delay t_r consists of two phases. It starts from the radial diffusion in interdisc spaces. Then, during the generation of a single-photon response, the decline in the cGMP concentration at the outer membrane should spread along the outer segment. In rods, the excitation may spread along tens of discs, which, in addition, form a baffling system for the diffusion. This might markedly contribute to the delay. However, the longitudinal diffusion is significant only at weak stimuli (a few photons per rod). At the intensities used in the present experiments (tens of photons per each disc), the reduction of cGMP in the outer segment is virtually uniform, and the longitudinal diffusion can be neglected [3].

The radial diffusion in the interdisc spaces of rods is usually considered to be very fast [3,15,25-27]. However, the only direct experimental evidence for this is the result in [25] where the temporal resolution, a few hundred milliseconds, was not sufficiently high to make any conclusion on the less than or equal to 10 ms time scale. If the radial diffusion were the source of the delay, it is expected that the delay would be longer the bigger the diameter of the ROS. Thus, it could be predicted that in frog rods of approximately 7-µm diameter the delay would be greater than five times longer than in fish rods whose diameter is less than or equal to 3 µm ($(7/3)^2 = 5.4$). This is not the case, though. In both species, the delay is virtually the same, approximately 10 ms (fish [17], frog, present paper). An estimate of the radial diffusion time can be obtained from the crude model shown in Figure 8. In darkness, the concentration of cGMP in the interdisc spaces and in the gap l between the disk rim and the plasma membrane is uniform. A bright flash leads to a virtually instantaneous drop in the GMP concentration in the cytoplasm between the discs to a new steady low level. The time course of the decrease in the near-channel concentration is determined by the diffusion equilibration of the gap l with the light-produced sink on the

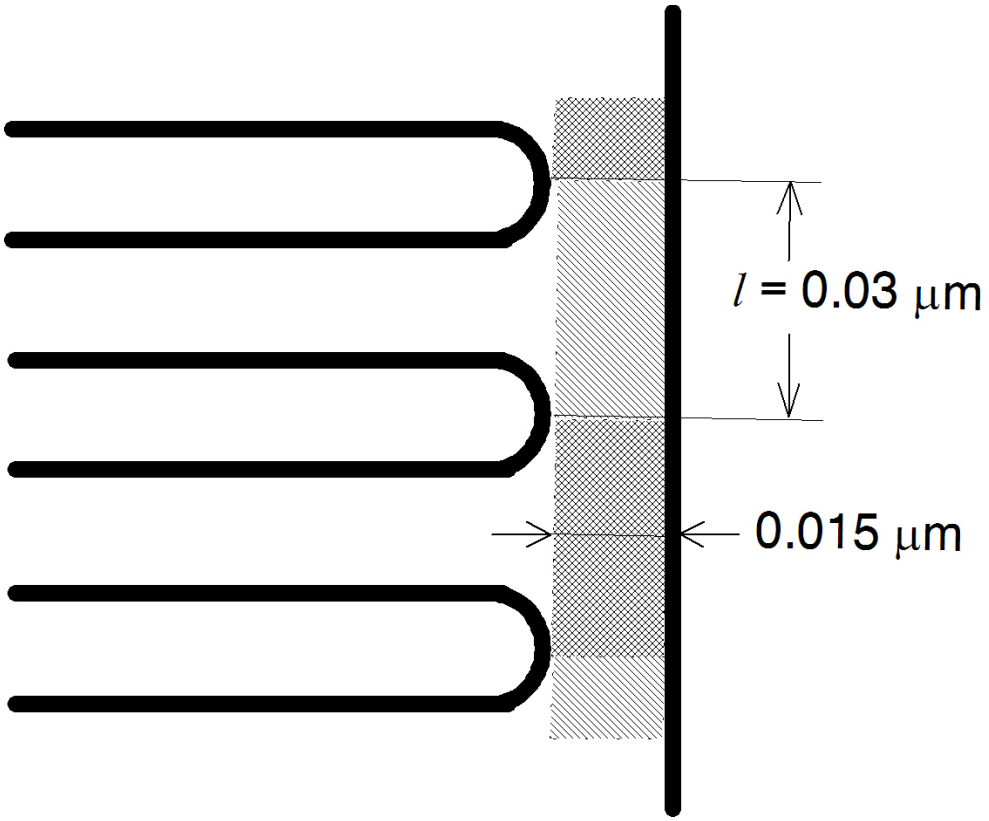

Figure 8. Schematics of the relationship between the rims of the photoreceptor disks and the plasma membrane. The dashed areas should be emptied by diffusion to close the cGMP-gated ionic channels (CNGCs) in the plasma membrane. l = disc spacing is assumed to be a coarse estimate of the diffusion distance.

disc surface. The characteristic time of equilibration is $t = l^2/D$ ([28], Equation 2.67). Assuming the diffusion constant for cGMP in the cytoplasm $D = 40$ μm^{2}s^{-1} [12,26,27,29] and $l = 0.03$ μm, one obtains that the concentration of cGMP at the plasma membrane drops to 0.5 of the dark level in 8.5 s^{-6} which is negligible compared to the experimental delay.

The next possible candidates are cGMP buffering and the release of cGMP from the ionic channels of the plasma membrane. Both processes are supposed to be fast [3]. It is found that the interaction of cGMP with channels takes milliseconds, possibly approximately 1 ms [30]. However fast, this may comprise a substantial part of the delay in cones. In rods, it can be neglected. This means that the main component of the transduction delay resides in the amplification cascade itself.

Stochastic modeling shows that an appropriate candidate for the delay-setting stage(s) is the dissociation of $T_{\alpha\beta\gamma}GTP$ into $T_{\alpha}GTP$ and $T_{\beta\gamma}$, and $T_{\alpha}GTP–PDE$ binding (Figure 4). To test this idea, we used a mathematical model of the photoresponse that included a detailed description of the activation chain between the photon absorption and formation of PDE* (E-MEM, see the Equations section). The model was fit to a cone response (Figure 7B), and then the time constants t_1 ... t_4 and t_5... t_6 were varied to test their effect on the phototransduction delay. Changing the time of the limiting step (t_1) between approximately 2.5 and 10 ms, as expected, resulted in inversely proportional changes in amplification (and thus, the response amplitude). Correspondingly, the delay as defined above decreased, although by only approximately 1 ms (inset in Figure 9A). However, the responses become virtually congruent after normalizing to their peaks and show no noticeable effect on the delay (Figure 9A). In contrast, similar variations in the time of the T*–PDE interaction (t_6) had virtually no effect on amplification but substantially changed the delay (Figure 9B).

Thus, contrary to intuition, the average duration of the cycle of T*–PDE* production does not significantly contribute to the photoresponse delay. Instead, the delay occurs at the stage of transmitting the signal from the activation cycle via T* to PDE.

PDE activation: A paradox: The short transduction delay in cones poses an important problem. We argue that the limiting step in T* production is the formation of the R*–$T_{\alpha\beta\gamma}$GDP complex; that is, t_{cycle} is approximately t_1. The rate of the process can be expressed as

Equation 3

$$v_{RG} = 1/t_{cycle} \approx 1/t_1 = c_e \cdot v_{enc}$$

Here, v_{enc} is the frequency of the diffusion encounters between single R* and Ts, and c_e is the efficiency of the encounters, that is, the fraction of encounters that lead to formation of R*–$T_{\alpha\beta\gamma}$GDP. v_{enc} is approximately 6,000 s^{-1} [3,4], and v_{RG} is approximately 200 s^{-1}; thus, c_e is approximately 1/30. v_{enc} is proportional to the surface packing density of T in the photoreceptor membrane, approximately 2,500 μm^{-2}. The surface packing density of PDE in amphibian rods is approximately 200 catalytic subunits μm^{-2}, that is, more than an order the magnitude lower than that of T [3]. Thus, if c_e of the T*–PDE collisions were the same as that of R* and T, then the rate of PDE activation by T* ($1/t_6$, Figure 2) should be 12 times lower than v_{RG}. The E-MEM shows that the delay in the rods (10 to 15 ms, Figure 3 and Figure 8) can be reproduced by $1/t_6$ approximately 20 s^{-1} which is ten times slower than the rate of the R*–T interaction ($1/t_1$ is approximately 200 s^{-1}, Table 2). This result is in coarse agreement with the idea that the overall efficiencies of the R*–T and T*–PDE interaction are approximately the same, at least in rods.

However, the transduction delay in cones is approximately three times shorter than that in rods (Table 1). Modeling shows that this delay is compatible only with $1/t_6$ greater than or equal to 200 s^{-1} which approximately equal to v_{RG} (Table 2, compared with $1/t_6$ = 20 s^{-1} in rods). It is believed that the PDE:T surface packing density ratio in cones is approximately the same as in rods (approximately 1:12 [3,7]) although in mammalian cones it could be two times higher (1:6 [31]). Then the question arises, how is it possible that in cones either v_{enc} or c_e at the T*–PDE interaction stage is six to 12 times higher than in rods.

Equations:

Deterministic description of the activation of the cascade and a complete model of the photoresponse—The average of many stochastic simulations is equivalent to the solution of a set of deterministic differential equations each describing the corresponding reaction [11]. Thus, to quantitatively analyze the factors that shape the phototransduction delay, we used an updated version of our MEM of phototransduction [14]. In the MEM, activation of PDE by R* is considered a single-step reaction with the (average) rate constant v_{RE}. The phototransduction delay in the MEM is implemented as an adjustable pure delay between the real and model stimuli. To account for the multistep activation of PDE responsible for the delay, we constructed an extended MEM (E-MEM) by including in the MEM 11 extra differential

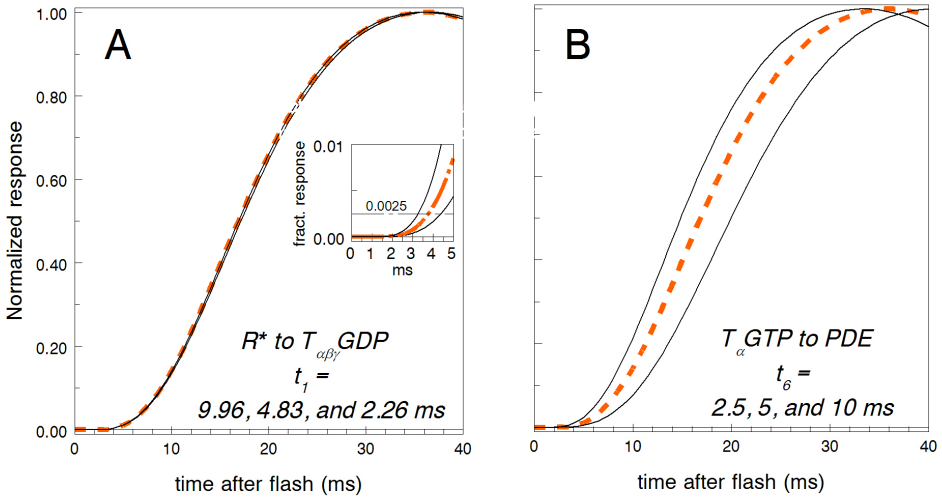

Figure 9. Effect of various activation steps on the photocurrent response delay. In all panels, the red dashed line is the best fit taken from the model of Figure 7B. In the main panels **A** and **B**, each response is normalized to unit at its peak. **A**: The duration of the R*–T activation cycle was changed twofold either way from the optimum value by changing the time-limiting step t_1 while keeping t_2, t_3, and t_4 constant at 0.1 ms. In the insert, the initial phase of the responses is shown on an expanded scale, and the responses are presented as fractional, that is, normalized to the saturated response. It is seen that the formally defined delay (time of crossing the criterion level) changes by about 1 ms when the duration of the activation cycle varies between 2.5 and 10 ms. If the responses are scaled to unit at their peaks (main panel **A**), the resulting curves are virtually congruent. They do not exhibit any noticeable shift along the time axis. **B**: The twofold variation in the time of $T_\alpha GTP$ and phosphodiesterase (PDE) interaction (t_6) greatly changed the delay. Only the time of less than or equal to 5 ms was consistent with the observed cone response. The non-normalized amplitude of the response in **B** does not perceptibly change when t_6 is varied.

equations describing steps 0 to 6 in the scheme Figure 1 (similar but not identical to those used in [15]). Now the rate of PDE activation v_{RE} is given by the output of Equation (7e), and in the absence of turn-off reactions steady $v_{RE} = 1/(t_1 + t_2 + t_3 + t_4)$. Hamer et al. [15] considered R*–TGDP binding and GDP release from the R* TGDP complex as reversible (their Equations A3a and A3b) while we treat them as irreversible transitions (our Equations (2e) and (3e)). This has no visible effect on the results.

Equation 1e

$$\frac{dR^*}{dt} = \frac{R}{t_0} - \frac{R^*}{t_1} + \frac{R^*T_{\alpha\beta\gamma}GTP}{t_4} - \frac{R^*}{t_p}$$

Equation 2e

$$\frac{d(R^*T_{\alpha\beta\gamma}GDP)}{dt} = \frac{R^*}{t_1} - \frac{R^*T_{\alpha\beta\gamma}GDP}{t_2}$$

Equation 3e

$$\frac{d(R^*T_{\alpha\beta\gamma})}{dt} = \frac{R^*T_{\alpha\beta\gamma}GDP}{t_2} - \frac{R^*T_{\alpha\beta\gamma}}{t_3}$$

Equation 4e

$$\frac{d(R^*T_{\alpha\beta\gamma}GTP)}{dt} = \frac{R^*T_{\alpha\beta\gamma}}{t_3} - \frac{R^*T_{\alpha\beta\gamma}GTP}{t_4}$$

Equation 5e

$$\frac{dT_{\alpha\beta\gamma}GTP}{dt} = \frac{R^*T_{\alpha\beta\gamma}GTP}{t_4} - \frac{T_{\alpha\beta\gamma}GTP}{t_5} + \frac{RpT_{\alpha\beta\gamma}GTP}{t_4}$$

Equation 6e

$$\frac{T_\alpha GTP}{dt} = \frac{T_{\alpha\beta\gamma}GTP}{t_5} - \frac{T_\alpha GTP}{t_6}$$

Equation 7e

$$\frac{dPDE^*}{dt} = \frac{T_\alpha GTP}{t_6} - \frac{PDE^*}{t_E}$$

Equation 8e

$$\frac{dRp}{dt} = \frac{R^*}{t_p} + \frac{RpT_{\alpha\beta\gamma}GTP}{t_4} - \frac{Rp}{t_{Ar}} - \frac{aAr \cdot Rp}{t_1}$$

Equation 9e

$$\frac{dRpT_{\alpha\beta\gamma}GDP}{dt} = \frac{aAr \cdot Rp}{t_1} - \frac{RpT_{\alpha\beta\gamma}GDP}{t_2}$$

Equation 10e

$$\frac{dRpT_{\alpha\beta\gamma}}{dt} = \frac{RpT_{\alpha\beta\gamma}GDP}{t_2} - \frac{RpT_{\alpha\beta\gamma}}{t_3}$$

Equation 11e

$$\frac{dRpT_{\alpha\beta\gamma}GTP}{dt} = \frac{RpT_{\alpha\beta\gamma}}{t_3} - \frac{RpT_{\alpha\beta\gamma}GTP}{t_4}$$

Here the parameters t_0 to t_6 correspond to those in Figure 1. t_P is the time constant of R* phosphorylation by rhodopsin kinase, t_{Ar} is the time constant of binding of phosphorylated rhodopsin by arrestin, and k_E is the time constant of the PDE* turn-off by the GAP complex, as in [14]. The pure delay between the real and model stimuli was set to 0, and proper fit to the initial phase of the response was achieved by varying t_0 to t_6.

ACKNOWLEDGMENTS

The authors declare no conflict of interest. This work was supported by grant # 15–04–03726 from the Russian Foundation for Basic Research to VG. Preliminary results were presented at the 15th International Conference on Vision (Visionarium-XV, Tvärminne, Finland, 2016).

REFERENCES

1. Lamb TD, Pugh EN Jr. A quantitative account of the activation steps involved in phototransduction in amphibian photoreceptors. J Physiol 1992; 449:719-58. [PMID: 1326052].
2. Pugh EN Jr, Lamb TD. Amplification and kinetics of the activation steps in phototransduction. Biochim Biophys Acta 1993; 1141:111-49. [PMID: 8382952].
3. Pugh EN Jr, Lamb TD. Phototransduction in vertebrate rods and cones: molecular mechanisms of amplification, recovery and light adaptation. In: Stavenga DG, Pugh EN Jr., de Grip WJ, editors. Handbook of Biological Physics. New York: Elsevier Science; 2000. p. 183–255.
4. Lamb TD. Biophys J 1994; 67:1439-54. Stochastic Simulation of Activation in the G-Protein Cascade of Phototransduction. [PMID: 7819482].
5. Liu Y-T, Matte SL, Corbin JD, Francis SH, Cote RH. Probing the Catalytic Sites and Activation Mechanism of Photoreceptor Phosphodiesterase Using Radiolabeled

Phosphodiesterase Inhibitors. THE JOURNAL OF BIOLOGICAL CHEMISTRY VOL. 2009; 284:31541-7. [PMID: 19758990].

6. Muradov H, Boyd KK, Artemyev NO. PDE6B Subunits Are Enzymatically Equivalent. J Biol Chem 2010; 285:39828-34. [PMID: 20940301].
7. Tachibanaki S, Tsushima S, Kawamura S. Low amplification and fast visual pigment phosphorylation as mechanisms characterizing cone photoresponses. Proc Natl Acad Sci USA 2001; 98:14044-9. [PMID: 11707584].
8. Astakhova LA, Firsov ML, Govardovskii VI. Kinetics of turnoffs of frog rod phototransduction cascade. J Gen Physiol 2008; 132:587-604. [PMID: 18955597].
9. Astakhova LA, Samoiliuk EV, Govardovskii VI, Firsov ML. cAMP controls rod photoreceptor sensitivity via multiple targets in the phototransduction cascade. J Gen Physiol 2012; 140:421-33. [PMID: 23008435].
10. Baylor DA, Lamb TD, Yau KW. The membrane current of single rod outer segments. J Physiol 1979; 288:589-611. [PMID: 112242].
11. Gillespie DT. Exact Stochastic Simulation of Coupled Chemical Reactions. J Phys Chem 1977; 81:2340-61. .
12. Lamb TD, Kraft TW. Quantitative modeling of the molecular steps underlying shut-off of rhodopsin activity in rod phototransduction. Mol Vis 2016; 22:674-96. .
13. Bisegna P, Caruso G, Andreucci D, Shen L, Gurevich VV, Hamm HE, DiBenedetto E. Diffusion of the second messengers in the cytoplasm acts as a variability suppressor of the single photon response in vertebrate phototransduction. Biophys J 2008; 94:3363-83. [PMID: 18400950].
14. Astakhova LA, Firsov ML, Govardovskii VI. Activation and quenching of the phototransduction cascade in retinal cones as inferred from electrophysiology and mathematical modeling. Mol Vis 2015; 21:244-[PMID: 25866462].
15. Hamer RD, Nicholas SC, Tranchina D, Lamb TD, Jarvinen JL. Toward a unified model of vertebrate rod phototransduction. Vis Neurosci 2005; 22:417-36. [PMID: 16212700].
16. Koshitani Y, Tachibanaki S, Kawamura S. Quantitative aspects of cGMP phosphodiesterase activation in carp rods and cones. J Biol Chem 2014; 289:2651-7. [PMID: 24344136].
17. Kawakami N, Kawamura S. Difference in the gain in the phototransduction cascade between rods and cones in carp. J Neurosci 2014; 34:14682-6. [PMID: 25355220].
18. Baumann C. The formation of metarhodopsin380 in the retinal rods of the frog. J Physiol 1976; 259:357-66. [PMID: 1085360].
19. Firsov ML, Govardovskii VI. Kinetics of Meta I – Meta II transition during the photolysis of rod and cone visual pigments in cold-blooded and warm-blooded vertebrates. Sens Syst 1988; 2:10-6. In Russian.
20. Leskov IB, Klenchin VA, Handy JW, Whitlock GG, Govardovskii VI, Bownds MD, Lamb TD, Pugh EN Jr, Arshavsky VY. The gain of rod phototransduction: reconciliation of biochemical and electrophysiological measurements. Neuron 2000; 27:525-37. [PMID: 11055435].
21. Cobbs WH, Pugh EN Jr. Kinetics and components of the flash photocurrent of isolated retinal rods of the larval salamander, *Ambystoma tigrinum*. J Physiol 1987; 394:529-72. [PMID: 2832596].
22. Hestrin S, Korenbrot JI. Activation kinetics of retinal cones and rods: Response to intense flashes of light. J Neurosci 1990; 10:1967-73. [PMID: 2355261].
23. Calvert PD, Govardovskii VI, Krasnoperova N, Anderson RE, Lem J, Makino CL. Membrane protein diffusion sets the speed of rod phototransduction. Nature 2001; 411:90-4. [PMID: 11333983].
24. Sokolov M, Lyubarsky AL, Strissel KJ, Savchenko AB, Govardovskii VI, Pugh EN, Arshavsky VY. Massive light-driven translocation of transducin between the two major compartments of rod cells: a novel mechanism of light adaptation. Neuron 2002; 34:95-106. [PMID: 11931744].
25. Lamb TD, McNaughton PA, Yau KW. Spatial spread of activation and background desensitization in toad rod outer segments. J Physiol 1981; 319:463-96. [PMID: 6798202].
26. Caruso G, Bisegna P, Shen L, Andreucci D, Hamm HE, DiBenedetto E. Modeling the Role of Incisures in Vertebrate Phototransduction. Biophys J 2006; 91:1192-212. [PMID: 16714347].
27. Gross OP, Pugh EN Jr, Burns ME. Spatiotemporal cGMP Dynamics in Living Mouse Rods. Biophys J 2012; 102:1775-84. [PMID: 22768933].
28. Clark J. The mathematics of diffusion. 2nd ed. Oxford: Oxford University Press; 1975.
29. Koutalos Y, Nakatani K, Yau KW. Cyclic GMP Diffusion Coefficient in Rod Photoreceptor Outer Segments. Biophys J 1995; 68:373-82. [PMID: 7536055].
30. Karpen JW, Zimmerman AL, Stryer L, Baylor DA. Gating kinetics of the cyclic-GMP-activated channel of retinal rods: Flash photolysis and voltage-jump studies. Proc Natl Acad Sci USA 1988; 85:1287-91. [PMID: 2448798].
31. Zhang X, Wensel TG, Kraft TW. GTPase regulators and photoresponses in cones of Eastern Chipmunk. J Neurosci 2003; 23:1287-97. [PMID: 12598617].

Articles are provided courtesy of Emory University and the Zhongshan Ophthalmic Center, Sun Yat-sen University, P.R. China. The print version of this article was created on 7 July 2017. This reflects all typographical corrections and errata to the article through that date. Details of any changes may be found in the online version of the article.